EJN
European Journal of Neuroscience

European Journal of Neuroscience, Vol. 27, pp. 3191–3204, 2008 doi:10.1111/j.1460-9568.2008.06292.x

Dynamic coupling of excitatory and inhibitory responses in the medial nucleus of the trapezoid body

Sandra Tolnai,[1,*] Bernhard Englitz,[1,2,*] Cornelia Kopp-Scheinpflug,[1] Susanne Dehmel,[1] Jürgen Jost[2] and Rudolf Rübsamen[1]
[1]Institute of Biology II, University of Leipzig, Talstr. 33, 04103 Leipzig, Germany
[2]Max-Planck-Institute for Mathematics in the Sciences, Inselstr. 22, 04103 Leipzig, Germany

Keywords: envelope coding, onset and ongoing latency, phase-locking, sideband inhibition, sinusoidal amplitude modulation (SAM)

Abstract

The neuronal representation of acoustic amplitude modulations is an important prerequisite for understanding the processing of natural sounds. We investigated this representation in the medial nucleus of the trapezoid body (MNTB) of the Mongolian gerbil using sinusoidal amplitude modulations (SAM). Depending on the SAM's carrier frequency (f_C) MNTB cells either increase or decrease their discharge rates, indicating underlying excitatory and inhibitory/suppressive mechanisms. As natural sounds typically are composed of multiple spectral components we investigated how stimuli containing two spectral components are represented in the MNTB, especially when they have opposing effects on the discharge rate. Three conditions were compared: SAM stimuli (1) with rate-increasing f_C, (2) with rate-increasing f_C and an additional unmodulated rate-decreasing pure tone, and (3) with rate-decreasing f_C and an unmodulated, rate-increasing pure tone. We found that responses under all three conditions showed comparable strength of phase-locking. Adding a rate-decreasing tone to a rate-increasing SAM increased phase-locking for modulation frequencies (f_{AM}) of ≤ 600 Hz. A comparison of two possible coding strategies – phase-locking vs. envelope reproduction – indicates that both strategies are realized to different degrees depending on the f_{AM}. We measured latencies for following modulations in rate-increasing and rate-decreasing SAMs using a modified reverse correlation approach. Although latencies varied between 2.5 and 5 ms between cells, a decrease in rate consistently followed an increase in rate with a delay of about 0.2 ms in each cell. These results suggest a temporally precise representation of rate-increasing and rate-decreasing stimuli at the level of the MNTB during dynamic stimulation.

Introduction

The medial nucleus of the trapezoid body (MNTB) is an integral source of tuned inhibition in the auditory brainstem providing glycinergic projections to the lateral and medial superior olives (LSO, MSO) (Glendenning *et al.*, 1981; Kuwabara & Zook, 1991; Kuwabara *et al.*, 1991; Banks & Smith, 1992; Sommer *et al.*, 1993). Although the general importance of the MNTB for sound source processing in LSO/MSO is commonly accepted (Brand *et al.*, 2002; for reviews see Yin, 2002; Tollin, 2003; Zhou *et al.*, 2005), the response properties of MNTB units when driven by complex stimuli, i.e. stimuli containing more than one spectral component, have not been investigated.

Even a simple acoustic stimulus, i.e. a pure tone, can either increase or reduce MNTB discharge rates depending on its frequency and intensity (Guinan *et al.*, 1972a; Sommer *et al.*, 1993; Tsuchitani, 1997; Smith *et al.*, 1998; Kopp-Scheinpflug *et al.*, 2003b; see also Fig. 1A). Increases in discharge rate are easily detectable, whereas reductions in discharge rate can only be observed in spontaneously active or acoustically driven units. These changes typically occur rapidly after stimulus onset and do not outlast the stimulus duration by more than the response latency. Such rate changes are already found in the afferents of MNTB neurons, the globular bushy cells of the cochlear nucleus, where they indicate the integration of excitatory and inhibitory inputs (Brownell, 1975; Martin & Dickson, 1983; Smith & Rhode, 1987; Spirou *et al.*, 1990). When increasing the frequency content of acoustic stimuli, rate reductions can additionally be caused by cochlear suppression (Pickles, 1988; Delgutte, 1990; Ruggero *et al.*, 1992; Rhode & Greenberg, 1994b) influencing the patterns of rate changes observed in subsequent stages of the auditory pathway.

In the case of the MNTB, it is still not clear whether stimulus-induced rate reductions result from the convergence of inhibitory and excitatory pathways onto MNTB principal cells or whether they are merely a reflection of the above mentioned rate reductions already effective at lower levels of the auditory pathway. If complex stimuli are considered, both cochlear suppression and neuronal inhibition targeting globular bushy cells might account for the latter. In favour of neuronal integration taking place at MNTB principal cells are several studies demonstrating the existence of inhibitory synapses targeting MNTB principal cells (Roberts & Ribak, 1987; Wenthold *et al.*, 1987; Adams & Mugnaini, 1990), and studies showing the effectiveness of GABA and glycine on MNTB neurons *in vitro* (Banks & Smith, 1992; Awatramani *et al.*, 2004, 2005).

Here we investigate responses of MNTB units to acoustic stimuli featuring more than one spectral component. We applied a similar paradigm as Moller (1975a) and Li *et al.* (2006), which entails the activation of combinations of rate-increasing and rate-reducing pure tones, with either one of the two being sinusoidally

Correspondence: Dr R. Rübsamen, as above.
E-mail: rueb@rz.uni-leipzig.de
*S.T. and B.E. contributed equally to this work.

Received 21 December 2007, revised 15 April 2008, accepted 27 April 2008

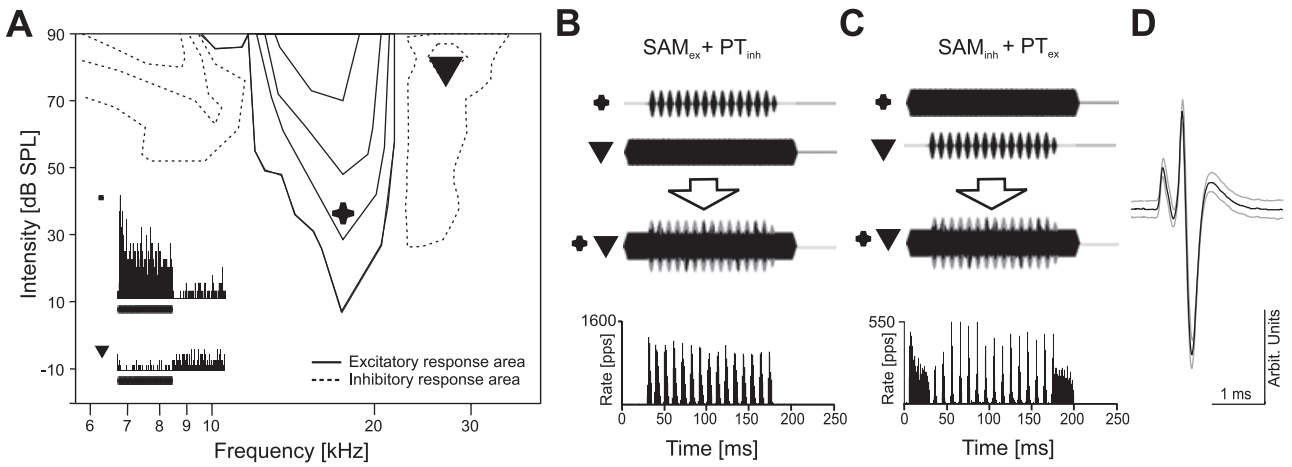

FIG. 1. Frequency response area of a typical MNTB neuron and stimulus paradigms. (A) Frequency response areas obtained under two-tone stimulation usually consist of an excitatory (solid) and one or more inhibitory regions (dashed). Excitatory and inhibitory frequency/intensity combinations used in the present two-tone stimulations are marked by the asterisk and the triangle, respectively. The excitatory signal is set at the unit's characteristic frequency (CF) 20 dB above threshold (i.e. 40 dB SPL). The inhibitory signal is set within the inhibitory sideband at 80 dB SPL. Insets show post-stimulus time histograms (PSTH) to 20 repetitions of the excitatory (top) and the inhibitory (bottom) pure tone, depicted below each histogram. (B) Two-tone stimulation paradigm for investigating the influence of sideband inhibition on temporal coding (top). The signal complex consists of an excitatory sinusoidally amplitude modulated signal (SAM$_{ex}$) and an inhibitory pure tone (PT$_{inh}$) (bottom). PSTH of a typical response to this composite stimulation with a modulation frequency (f_{AM}) of 100 Hz. Note the unit's periodic discharge pattern locking to the envelope of the f_{AM} and the lack of any discharge activity during the initial 25 ms of the stimulus when the signal only contains spectral energy in the unit's inhibitory sideband. (C) Two-tone stimulation paradigm for analyzing the dynamic properties of sideband inhibition. (top) The signal complex consists of an excitatory pure tone (PT$_{ex}$) and an inhibitory sinusoidally amplitude-modulated signal (SAM$_{inh}$) (bottom). PSTH of an exemplary response to this stimulation with f_{AM} = 100 Hz. The initial and final 25 ms resemble the phasic–tonic response to the PT$_{ex}$. From about 30 to 180 ms the unit's discharge activity is strongly modulated displaying ten peaks matching the periods of the SAM$_{inh}$. (D) Typical mean spike waveform (black) of an MNTB unit (gray: standard deviation).

amplitude-modulated. The aim of the study was to compare fidelity and timing of these opposing rate changes, i.e. to quantify temporal properties of excitation and inhibition at MNTB principal cells.

Methods

Twenty-five Mongolian gerbils (*Meriones unguiculatus*), aged between 2 and 4 months, were used in this study. All experimental procedures were approved by the Saxonian District Government, Leipzig and the ethical guidelines of the University of Leipzig. Surgical procedures were the same as described by Kopp-Scheinpflug *et al.* (2002). Briefly, animals were anesthetized during the surgery and recording procedure with a xylazine hydrochloride/ketamine hydrochloride mixture (Rompun®, Bayer, xylazine 0.006 mg/g body weight i.p.; Ketavet®, Upjohn, ketamine 0.13 mg/g body weight i.p. initial dose, one-third of the initial dose as supplementary s.c. when necessary). Animals were placed in a sound- and echo-attenuated booth (Type 400; Industrial Acoustic Company, Niederkrüchten, Germany) on a vibration-isolated table and fixed in a stereotaxic device using a metal bolt cemented on the dorsal surface of the skull. While recording, body temperature was maintained at ~37°C with a heating pad. The MNTB was approached dorsally with glass micropipettes (Harvard Apparatus) filled with 3 M KCl through a 500-μm-diameter hole drilled in a midline position into the occipital bone 2000–2300 μm caudal to the lambda suture.

Verification of recording sites

The location of recording sites was determined by physiological criteria: (1) the units were exited only to stimuli presented to the contralateral ear (Guinan *et al.*, 1972a,b), and (2) they were characterized by complex waveforms, i.e. the bipolar postsynaptic action potential was preceded by a monophasic prepotential indicating the discharge of the calyx of Held (Guinan *et al.*, 1972a; Guinan & Li, 1990; Wu & Kelly, 1992; Kopp-Scheinpflug *et al.*, 2003b). These two criteria combined with the MNTB-typical stereotaxic coordinates identified the units as principal cells of the MNTB and allowed a distinction from fibres and non-principal cells of this nucleus (Guinan *et al.*, 1972a; Guinan & Li, 1990; Wu & Kelly, 1992; Kopp-Scheinpflug *et al.*, 2003b). In 14 animals the recording sites were also verified histologically; in six animals horseradish peroxidase (HRP; Sigma, P6782) and in eight hydroxystilbamidine (FG; Biotium; equivalent to FluoroGold™) was injected iontophoretically (+ 1.5 μA/4–5 min) into the MNTB at the end of the recording session. The animals were allowed to survive for 24 h or 5 days following HRP or FG injections, respectively. They were then given a lethal dose of Na-pentobarbital (Narcoren®, Rhone Merieux, 100 mg/100 g body weight i.p.) and perfused via the left ventricle with normal saline and then fixed with paraformaldehyde (2.5%). The brains were removed from the skull and post-fixed in paraformaldehyde (4°C, 24 h), and thereafter embedded in agarose. Serial transverse sections (HRP, 10 μm; FG, 50 μm) were cut using a vibratome. HRP tissue sections (100 μm) were reacted using the 3,3′-diaminobenzidine (DAB) reaction to visualize the HRP mark (Adams, 1981). Sections were counterstained with cresyl violet, examined under the light microscope and the electrode tracks and recording sites were reconstructed. FG tissue sections were examined with a fluorescence microscope (Zeiss, Axioskop, absorption/emission, 361/536 nm).

Acoustic stimulation

Near-field acoustic stimuli were delivered through custom-made earphones (acoustic transducer: DT 770 pro, Beyerdynamic) fitted with plastic tubes (70 mm length, 5 mm diameter), which were inserted into the outer ear canal at a distance of ~4 mm to the

tympanic membrane. The frequency characteristic of the coupler was measured with a ¼-inch condenser microphone (Bruel & Kjaer type 2618) and used for correcting the signal output online to a maximum of 90 dB SPL (sound pressure level). Stimuli were digitally generated by a PC486/33 computer and delivered at 250 kilosamples/sec per channel through a two-channel, 14-bit D/A converter including a custom-made low-pass resynthesis filter (50 kHz cut off), and a software-controlled attenuator (0–120 dB in 1-dB steps).

Data collection

At the beginning of the recording session in each animal, the stereotaxic coordinates of the MNTB were determined by online analysis of acoustically evoked multi-unit activity using micropipettes with impedances of < 7 MΩ. Differentiation of the MNTB from other nuclei within the superior olivary complex (SOC) was facilitated by the fact that MNTB units are driven exclusively by stimuli presented to the contralateral ear. Extracellular recordings from single units were obtained with high-impedance micropipettes (10–30 MΩ). The activity of isolated single-units was band pass filtered (0.45–7 kHz). The amplified signals were delivered to a spike discriminator (SD 1; Tucker Davis Technologies) followed by an event-timer PC interface. Events were acquired with 10-μs resolution.

When a single unit was isolated its excitatory response area to stimulation of the contralateral ear was measured by presenting pure tone bursts (100 ms duration, 5 ms linear rise fall time, 200 ms recording interval) within a pre-defined array of 16×15 frequency/intensity pairs. Each frequency/intensity combination was presented three or five times in pseudo-random order. Spontaneous activity was acquired in silent runs interspersed with the stimulus runs. A single unit's inhibitory response area was established by means of two-tone stimulation, i.e. in addition to tone bursts of varying frequency/intensity combinations, an additional pure tone at the unit's characteristic frequency (CF) was presented to the same ear (100 ms duration, 5 ms rise fall time, 10–20 dB above unit's threshold). Inhibitory response areas were then seen as reductions of responses evoked by stimulation at the CF (an example of a unit's excitatory and inhibitory response areas is shown in Fig. 1A; for further details of the acquisition of response areas see Kopp-Scheinpflug *et al.*, 2002). The question of whether this reduction is of suppressive or inhibitory kind is detailed in the discussion. In the meantime, a reduction in firing rate is termed inhibition.

Responses to sinusoidal amplitude-modulated (SAM) signals were recorded under three conditions: (1) with the carrier frequency at the unit's CF, (2) with the carrier frequency at the unit's CF and an additional unmodulated pure tone with a frequency within the center of the inhibitory sideband, and (3) with the carrier frequency at a frequency within the center of the inhibitory sideband and an unmodulated pure tone at the unit's CF (Fig. 1). SAM signals had a duration of 150 ms with a 5-ms rise/fall time starting 25 ms after the recording onset (recording interval, 250 ms). The optional unmodulated pure tone started at 0 ms (with the onset of the recording interval) and lasted for 200 ms, i.e. it outlasted the SAM signal by 25 ms (Fig. 1B and C).

All SAM signals were 100% modulated and had modulation frequencies (f_{AM}) ranging from 20 to 1000 Hz (20, 50, 100–1000 in steps of 100 Hz; for units with CFs < 2 kHz: maximum f_{AM} = 0.5 CF). Both SAM signals and pure tones were presented to the contralateral ear. CF signals had levels of 15–70 dB SPL. Signals with a frequency within the center of the inhibitory sideband had levels of 65–85 dB SPL.

The temporal dynamics of the response to single-tone and two-tone stimuli were determined from post-stimulus time histograms (PSTHs). These were recorded by presenting 150 repetitions of (1) a 200-ms pure tone at the unit's CF at 80 dB SPL followed by 50 ms of silence and (2) in the case of two-tone experiments by presenting an additional pure tone with a frequency within the center of the inhibitory sideband at 80 dB SPL starting 25 ms after the first tone and lasting for 150 ms. If recordings could be acquired for long enough, the two-tone stimulation paradigm was repeated for multiple intensities (between 30 and 90 dB SPL). Data will be referred to as single-tone/two-tone PSTH in the following.

Data evaluation and analysis

Spike recordings were visualized by PSTH. The effects of SAM stimulation were illustrated by period histograms, in which spikes recorded at a given envelope phase during all modulation cycles of a stimulus were accumulated and plotted. Estimation of post-stimulus response dynamics from the PSTH was aided by the BARS (Bayesian adaptive regression splines) algorithm (Kass *et al.*, 2005), which can both follow rapid changes in the PSTH as well as smooth its tonic parts. Using this method, average discharge rates, peak widths and time of half-maximal activation/reduction could be measured more objectively and automatically.

Excitatory and inhibitory response latencies were measured both from single-tone/two-tone PSTH and from SAM PSTH. In single/two-tone experiments, latencies were quantified by the time of half-maximal activation/reduction (HA/HR; onset latency) (Kopp-Scheinpflug *et al.*, 2003b). The criterion of half-maximal, i.e. 50%, activation/reduction was chosen as here the typically steep slope provided accurate measurements. Although other criteria in the vicinity of 50% would have given equally accurate measurements, much greater variability would have resulted for exceedingly high or low criteria. Importantly, onset latencies (i.e. response to a stimulus after silence) were shown to be dependent on the stimulus intensity (Moller, 1975b; Joris & Yin, 1992). The present results show a wide spread of latencies ranging from 2.5 ms to more than 8 ms (Fig. 2C, open circles). Equivalent level-dependencies have to be expected for the inhibitory onset latencies. As the relationship between the onset latencies for excitation and inhibition are not known, a comparative analysis would face the problem of choosing corresponding stimulus levels for excitation and inhibition.

To overcome this problem we based the analysis of excitatory and inhibitory response latencies on the periodic cross correlation (PCC) method, a modified reverse correlation method (Fig. 2A and B), which measures the ongoing latency during continuous stimulation, i.e. the response to changes in the stimulus (in the present study: changes in level). Similar to the classical reverse-correlation method (in conjunction with random amplitude modulation (AM)s, e.g. Moller, 1976) it has the advantage of using information of the entire stimulus-evoked response, leading to quite narrow distributions of latency values and exceedingly small standard deviations for individual cells (see Results).

First, the cross correlation between the SAM envelope and the resulting PSTH was computed for each f_{AM} tested. Maxima in each cross correlation correspond to ongoing latencies of best agreement between stimulus envelope and response PSTH. As the stimuli are periodic, the cross correlations are also periodic. Then, to select the maximum corresponding to the actual ongoing latency, multiple cross correlations for different f_{AM}s were superimposed. The ongoing latency at which most maxima aligned was taken to be the actual ongoing latency. More precisely, to construct a smoothed histogram of the positions of the maxima, each maximum's position was convolved with

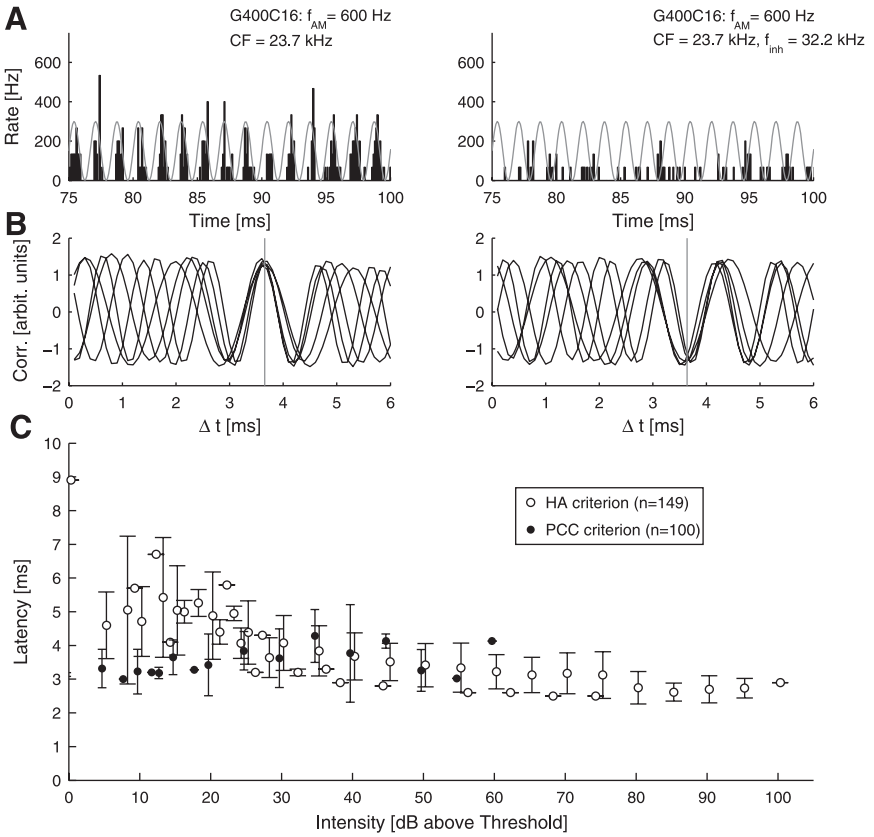

FIG. 2. Illustration of the periodic cross correlation (PCC) method for the measurement of ongoing latency and comparison to onset latencies obtained by the half-activation (HA) method. (A) The stimulus envelope (gray) and the resulting response PSTH (black) are shown superimposed for SAM_{ex} (left) and SAM_{inh} + PT_{ex} (right). In both cases the correct latency is not obvious by simple comparison of the envelopes. (B) Superposition of normalized cross correlations of the stimulus envelope with the response PSTH at a number of f_{AM}. Clearly, an optimal overlap is established at 3.7 ms (vertical gray line) for both SAM_{ex} (left, maxima) and SAM_{inh} + PT_{ex} (right, minima). (C) Comparison of ongoing and onset latencies determined by PCC (filled circles) and HA (open circles) methods shows that ongoing latencies are less variable for low stimulus levels and less dependent on the stimulus level. Note that levels are given with respect to each unit's threshold, as this scaling leads to more consistent results across units than absolute levels.

a Gaussian kernel (SD 0.3 ms, choice of kernel shape and width were not critical) and the resulting vectors were summed. The maximum of the resulting vector was taken as an indication of the actual ongoing latency. In the case of SAM carrier frequencies placed into the center of the inhibitory sideband, the same method was applied with the only difference of using minima instead of maxima, which corresponds to matching the peaks in the stimulus envelope with the troughs in the response PSTH. Only f_{AM}s ≥ 600 Hz were used, as the reduced presence of a (periodic) onset response led to a precise overlap of the correlation maxima/minima (within 0.2 ms, Fig. 2B).

The level of phase-locking to the envelope of an SAM stimulus was quantified using the vector strength (VS; Goldberg & Brown, 1969), defined as:

$$\mathrm{VS} = \left[\sqrt{\left[\sum_{\text{spikes}} \cos(\alpha)\right]^2 + \left[\sum_{\text{spikes}} \sin(\alpha)\right]^2}\right] \Big/ n$$

where the sum runs over spikes recorded between 20 and 150 ms after stimulus onset, α denotes the phase of each spike with respect to the envelope period of the stimulus and n is the total number of spikes. The VS value quantifies phase-locking by assessing the degree of clustering of spike times around a single phase after wrapping them by the stimulus period. A VS value of 1 indicates perfect phase-locking, i.e. all spikes occur at exactly the same phase of the stimulus envelope. As pointed out previously (Rhode & Greenberg, 1994a) the interpretation of the VS depends on the stimulus shape used. Each stimulus shape has an associated VS value, which is computed analogously to the VS of the response, e.g. for a sinusoidal envelope the VS = 0.5. If the response shape matches the stimulus shape, their corresponding VS values agree. However, the reverse is not necessarily true, rendering the VS inadequate for distinguishing moderate phase-locking from stimulus reproduction. In the text we use the term 'to follow the envelope' to indicate VS values significantly > 0. The term 'phase-locking' is only used if the VS values exceed 0.5 – the VS value of the stimulus. Significant deviation from 0 was tested based on the Rayleigh approximation (Greenwood & Durand, 1955; Knipschild *et al.*, 1992), which provides significance bounds for the VS values under the 0-hypothesis of an unmodulated response for a given sample size.

To assess stimulus reproduction we quantified the distance between the stimulus envelope S and the response PSTH R by their normalized correlation. This requires shifting the response forward by the cell's ongoing latency τ (as determined by the PCC method), in order to compare corresponding times of stimulus and response. As our stimulus is periodic, it is sufficient to compute the correlation over one stimulus period T. The corresponding formula:

$$\mathrm{Corr}_{\mathrm{norm}}(S(t), R(t-\tau)) \equiv \frac{1}{\|S\| \cdot \|R\|} \sum_{t=0}^{T} S(t) R(t-\tau)$$

will be abbreviated $Corr_{norm}$ in the text. Here, $||S||$ and $||R||$ denote the Euclidean norm of S and R, viewed as time-binned vectors. Dividing by them makes the $Corr_{norm}$ values independent of the stimulus intensity or the average firing rate of the response. To evaluate the results of this method, it is important to keep some of the characteristics of S and R in mind. Both S and R are positive (positive sound pressure and positive firing rate), and thus not all correlation values in the range of −1 to 1 are attainable (only products of positive values in the sum). Thus, the $Corr_{norm}$ values are limited to the positive range [0,1], e.g. an unmodulated response has a value of 0.82 when compared with the sinusoidal envelope of the stimulus. Very low $Corr_{norm}$ values (< 0.5) would only be attained if the response occurred out of phase compared with the stimulus envelope, which is unlikely to occur in the following as the ongoing latency has already been corrected for. Very high values (> 0.9) will only be attained if the response shape approaches the stimulus envelope shape.

Further, the shape of each period histogram was analysed by quantifying its symmetry via the location of the maximum with respect to the overall period histogram. More precisely, the period histogram was first smoothed by averaging over neighboring points in the histogram (in a 2% radius), then phase-shifted to start with its minimum. Next, the leftmost and rightmost bins (each containing 2.5% of the histogram's mass) of the period histogram were removed, reducing the histogram to its central section, whose symmetry was to be quantified. Finally, the position of the maximum was linearly normalized with respect to the total length of the capped period histogram, where −1 indicates that the maximum was at the very beginning, 0 at the middle and 1 at the very end of the capped period histogram. Hence, a monophasic, symmetric response would receive a value of 0. This measure will be termed maximum asymmetry (MA) in the text.

For most analyses the contribution of the steady-state response was analysed by excluding the first 20 ms of the response. Data analysis and statistical comparisons were performed using custom-written software in MATLAB 7.1 (The Mathworks, Nattick, MA, USA). Error bars in figures represent one standard error of the mean (SEM). If the 0-hypotheses of Gaussianity (Kolmogorov–Smirnov test) and equal variances (*F*-test) could not be rejected, the single- or two-group (paired or unpaired) *t*-test was applied, otherwise significance was assessed using the Wilcoxon signed rank test (one group) or the Mann–Whitney rank sum test (two groups).

Results

Extracellular recordings were obtained from 149 principal cells in the MNTB of 25 Mongolian gerbils. These were characterized by complex spike waveforms composed of a monophasic positive potential (prepotential) followed by a biphasic action potential (Fig. 1D). All units were solely driven by stimulation of the contralateral ear. PSTHs mostly showed a primary-like-with-notch response pattern, but also primary-like patterns were observed. Characteristic frequencies ranged from 0.5 to 46 kHz and thresholds from −10 to 60 dB SPL.

In the following sections, two aspects of the dynamic response properties to SAM stimuli will be analysed: phase-locking and envelope reproduction. In the third section response latencies of excitation and inhibition are compared.

Modulation transfer properties – phase-locking

Responses to temporally modulated stimuli

To investigate the temporal response properties, SAM tone bursts were presented to the contralateral ear at each unit's characteristic frequency (SAM_{ex}). Units responded to the SAM_{ex} stimulation with a periodically modulated firing rate, whose period length matched the period length of the stimulus f_{AM} (representative response: Fig. 3, top row). Quantification of phase-locking was based on calculation of the VS (see Methods) of spike discharges to 150 stimulus repetitions. In the following analysis 98 units were considered for which the whole range of modulation frequencies (20–1000 Hz) could be covered.

All units followed the envelope of the SAM signal or even phase-locked to a certain phase, although the fidelity of response synchronization varied in a frequency-specific manner. Most units had low pass or band pass modulation transfer functions based on the VS values (VS-MTFs). The mean VS-MTF had a band pass shape (Friedman test: $P << 0.001$), i.e. showed a gradual increase of the VS with increasing f_{AM} up to 300 Hz followed by a steady decrease (Fig. 4, A1). Towards higher f_{AM} the proportion of units that no longer showed significant VS values continuously increased. Regardless, about 95% of units (93/98) followed the SAM signal at a modulation rate of 1000 Hz. The maximal VS values varied between 0.41 and 0.94 (mean 0.71, SD 0.11). About 75% of the units (75/98) had their maximal VS values at f_{AM} ranging between 100 and 400 Hz (mean 0.71, SD 0.11). About 4% (4/98) had their maximal VS at f_{AM} < 100 Hz (mean 0.59, SD 0.08), and ∼20% of the units (19/98) showed their maximal VS (mean 0.71, SD 0.08) at f_{AM} > 400 Hz. These differences considered, the data still indicate a high degree of consistency of responses of MNTB units to dynamically altered sound amplitudes.

Rate-based MTFs yielded a less uniform characterization of the MNTB units (analysis not shown), e.g. band pass or low pass characteristics. The mean rate-based MTF had a band pass shape (see Fig. 8, open circles). The maximum discharge rates to SAM stimuli did not covary with the units' CFs.

Influence of inhibition on response modulation

The effect of acoustically evoked inhibition on temporal acuity of the responses to SAM was investigated in 38 units by applying a composite stimulation paradigm termed $SAM_{ex} + PT_{inh}$: SAM signals were presented at the unit's CF between 15 and 70 dB SPL, and an additional pure tone was added at the frequency/intensity combination that had caused the strongest inhibition devoid of any excitatory response in the respective units (0.2–1.8 octaves above CF; 45–85 dB SPL) (Fig. 1B). The f_{AM} was systematically varied between 20 and 1000 Hz. The inhibitory signal component preceded and outlasted the excitatory SAM by 25 ms to achieve a tonic level of inhibition into which the SAM excitation was embedded (Fig. 1B, bottom). The effect of inhibition on the excitatory modulation transfer properties was evaluated from the differences in the VS values obtained with and without PT_{inh}. As with the SAM_{ex} (Fig. 3, top row), the response PSTHs for the $SAM_{ex} + PT_{inh}$ stimulation were modulated in correspondence with the f_{AM} (Fig. 3, middle row).

In 30 units the whole range of f_{AM} could be covered for SAM_{ex} and $SAM_{ex} + PT_{inh}$ stimulation. Their CF ranged between 1.2 and 33.6 kHz and the thresholds from 10 to 50 dB SPL. All units phase-locked to amplitude modulations at the units' CFs in the presence of inhibitory sideband stimulation. The mean VS-MTF for $SAM_{ex} + PT_{inh}$ (Fig. 4, B1, filled circles) also showed a band pass characteristic. The VS values of SAM_{ex} and $SAM_{ex} + PT_{inh}$ differed significantly for $f_{AM} \leq 300$ Hz on the population level ($P < 0.01$, Mann–Whitney rank sum test) and for $f_{AM} \leq 600$ Hz on a cell-by-cell comparison ($P < 0.01$, Wilcoxon signed rank test, see Fig. 4, D1, black dots).

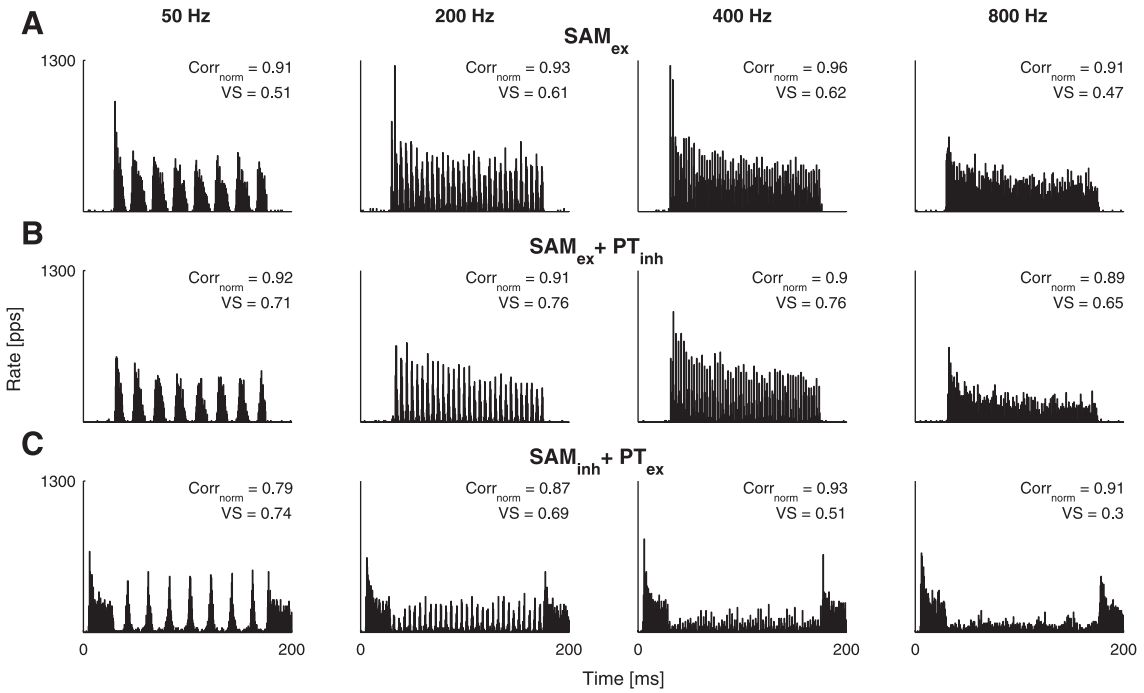

FIG. 3. PSTH of a single unit (unit G56923, CF = 21.0 kHz, threshold 25 dB SPL) in response to SAM tones for f_{AM} = 50, 200, 400 and 800 Hz under three different stimulus settings. (A) Responses to modulations at the unit's CF (SAM_{ex}), 10 dB above threshold (35 dB SPL). (B) Responses of the same unit to SAM signals at the unit's CF (35 dB SPL) combined with a pure tone with a frequency–intensity combination set into the inhibitory sideband (28.2 kHz, 60 dB SPL). Note the overall reduction in rate compared with the SAM_{ex} stimulation. (C) Responses to modulations of inhibitory sideband stimulation (28.2 kHz, 50 dB SPL) combined with pure tone stimulation at CF (20 dB SPL). In contrast to SAM_{ex} stimulation, stimulus response is maximal when stimulus intensity is minimal, i.e. response peaks occur anti-phasic to the SAM_{ex} conditions. The unit's excitatory and inhibitory ongoing latencies were 3.2 ms and 3.3 ms, respectively. The unit's excitatory and inhibitory onset latencies were 3.2 ms and 4.8 ms, respectively. VS and $Corr_{norm}$ values for each stimulus condition are displayed in the top right corner of the PSTHs.

The maximum VS values of SAM_{ex} + PT_{inh} were 0.58–0.87 (0.75, SD 0.08) at f_{AM} ranging from 50 to 700 Hz. Twenty-six of 30 units had higher maximum VS values with inhibitory sideband stimulation [0.58–0.87 (0.75, SD 0.08) compared with 0.54–0.85 (0.69, SD 0.09)] without inhibition.

Interspike interval (ISI) histograms of a unit under SAM_{ex} + PT_{inh} stimulation are shown in Fig. 5B. In comparison with SAM_{ex} stimulation (Fig. 5A), further ISI peaks appear which point to increased skipping of stimulus cycles in the neural responses. Additionally, the ISI peak around 1 ms is reduced, which indicates fewer spikes within one SAM period (separated only by the refractory time). Furthermore, up to 100 Hz of f_{AM} the second ISI peak is shifted to higher values, suggesting longer time spans between the last spike of a respective stimulus cycle and the first spike of the next cycle. Taken together, these results indicate a shortening of the time window for spike generation.

Next, we compared the period histograms between the SAM_{ex} and SAM_{ex} + PT_{inh} stimulation to see whether inhibition has an effect on the symmetry of the period histogram (Fig. 6). For quantification, MA values were calculated, which for monophasic and fully symmetric period histograms would have an MA = 0 (see Methods). Negative values indicate a dominance of the neuronal response before the histogram's center of mass, i.e. early occurrence of the main response peak, and positive values indicate a respective neuronal response after the histogram's center of mass, i.e. a late response peak. Representative period histograms with and without inhibitory sideband stimulation of a single unit are shown in Fig. 6A and B. Mean MA values for the population over the whole range of f_{AM} are shown in Fig. 6D. For either conditions the 0-hypothesis of centered peaks, i.e. symmetric period histograms, is not fulfilled for the whole range of tested f_{AM} ($P < 0.01$, Wilcoxon signed rank test).

The cell-by-cell difference in MA values of the period histograms between the SAM_{ex} and SAM_{ex} + PT_{inh} conditions (SAM_{ex} – SAM_{ex} + PT_{inh}) was significant for $f_{AM} \leq 400$ Hz ($P < 0.01$, Wilcoxon signed rank test, Fig. 6E). We consider this an indication for the PT_{inh} causing a higher symmetry of period histograms by reducing the onset discharge and consequently shifting the main peak to later times.

In all 30 units the stimulation with PT_{inh} led to an almost constant decrease in discharge rate over the whole range of f_{AM} (mean 51 pps, SD 5 pps). The shape of rate-based MTFs mostly remained unchanged under the SAM_{ex} + PT_{inh} condition; units had mostly band pass rate-based MTFs under either stimulus condition (see Fig. 8).

Dynamic properties of sideband inhibition

In 47 units the dynamic properties of acoustically evoked inhibition were measured with a different setting of composite stimulation: after determining a unit's inhibitory sidebands, pure tone signals were presented at the unit's CF (5–35 dB above threshold) which – when presented alone – generated a phasic–tonic discharge activity, i.e. an onset peak followed by a reduced, constant discharge activity. Then, SAM signals with the carrier frequency within the center of the high-frequency inhibitory sideband were added (Fig. 1C). The frequency of the SAM_{inh} was 0.2–1.8 octaves above the units' CFs, and the peak intensity 65–85 dB SPL. The motivation for this stimulus setting, termed SAM_{inh} + PT_{ex}, was as follows. Starting from the phasic–tonic excitatory response, the dynamics of acoustically evoked inhibition can be measured by relating the temporal characteristics of the

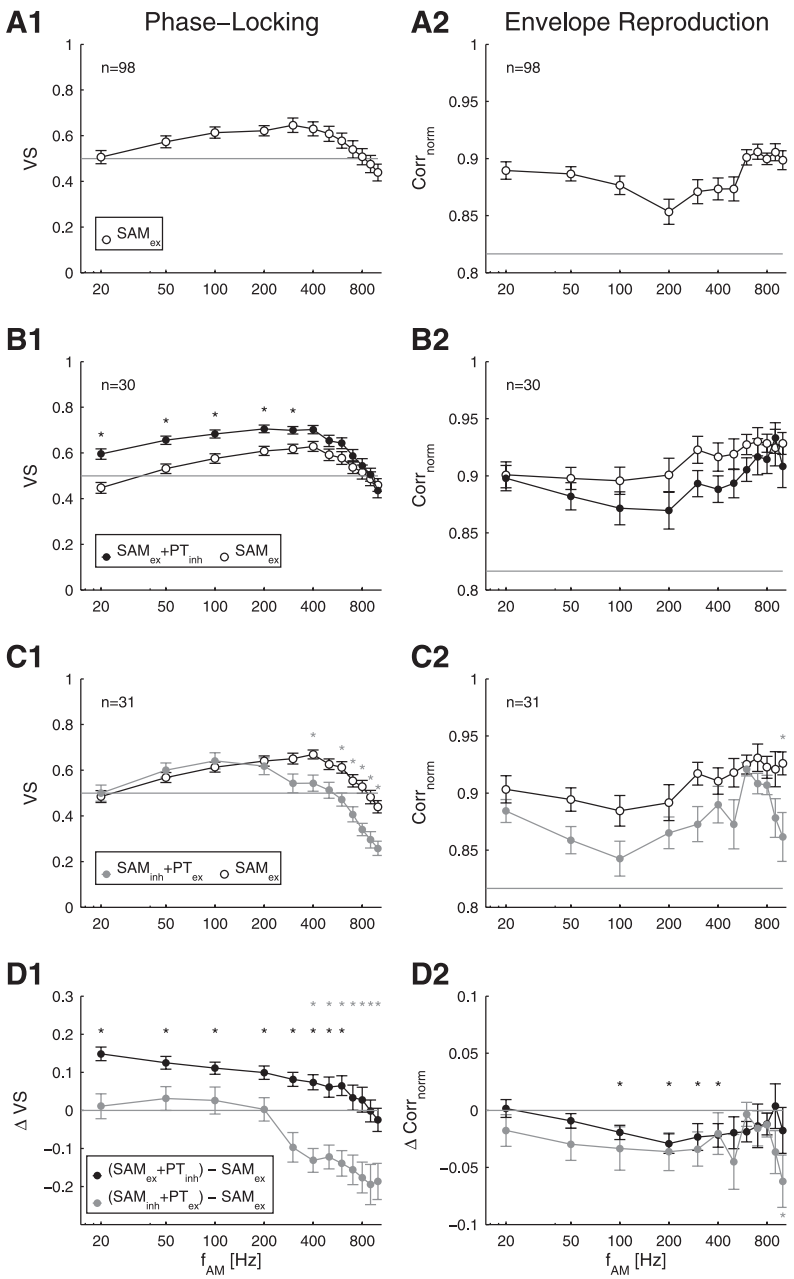

FIG. 4. Modulation transfer functions (MTFs) based on the vector strength (VS) (left column) and based on the normalized correlation ($Corr_{norm}$) between stimulus and response (right column). (A1) The mean VS-MTF of 98 MNTB units for modulations at units' CFs (SAM_{ex}) has a band pass characteristic albeit lacking a pronounced peak. (B1) Mean VS-MTFs of 30 units for modulations at units' CFs with (filled circles, $SAM_{ex} + PT_{inh}$) and without a pure tone placed into the inhibitory sideband (open circles, SAM_{ex}). The two conditions differ significantly for f_{AM} up to 300 Hz on the population level ($P < 0.01$) and up to 600 Hz on a cell-by-cell comparison ($P < 0.01$, see D1 black filled circles). (C1) Mean VS-MTFs of 31 units for modulations at units' CFs (open circles, SAM_{ex}) and for modulations placed into the inhibitory sideband (gray filled circles, $SAM_{inh} + PT_{ex}$). The two conditions differ significantly for $f_{AM} > 600$ Hz on the population level ($P < 0.01$) and for $f_{AM} > 400$ Hz on a cell-by-cell comparison ($P < 0.01$, see D1 gray filled circles). (A2) For SAM_{ex} the $Corr_{norm}$ MTFs take the course of an inverted band-pass function, thus showing the opposite dependence observed for the VS values. (B2) Comparison of $Corr_{norm}$ MTFs for SAM_{ex} (open circles) and $SAM_{ex} + PT_{inh}$ (filled circles). The inhibitory pure tone induces a consistent trend towards lower $Corr_{norm}$ values across the whole range of f_{AM}, which is significant on a cell-by-cell comparison in the range of 100–400 Hz ($P < 0.01$, see D2 black circles). (C2) Comparison of $Corr_{norm}$ MTFs for SAM_{ex} (open circles) and $SAM_{inh} + PT_{ex}$ (gray filled circles). The $Corr_{norm}$ MTFs for $SAM_{inh} + PT_{ex}$ show a consistent trend towards lower $Corr_{norm}$ values, which is, however, only significantly different for $f_{AM} = 1000$ Hz ($P < 0.01$). Data are shown as mean and SEM. The gray line in A1–C1 indicates the VS value of the stimulus; the gray line in A2–C2 indicates the $Corr_{norm}$ value of an unmodulated response. For population comparisons the Mann–Whitney rank sum test and for cell-by-cell comparisons the Wilcoxon signed rank test was applied. *$P < 0.01$.

inhibitory SAM stimulus to any dynamic changes of the tonic response component. Therefore, the PT_{ex} stimulus preceded the SAM_{inh} stimulus by 25 ms, which prevented interference with the unit's excitatory phasic-on component.

Representative responses to $SAM_{inh} + PT_{ex}$ stimulation for various f_{AM} are shown in Fig. 3C. When adding the SAM_{inh} stimulus the phasic–tonic response to the PT_{ex} changes to being periodically modulated, with the modulation frequency matching the stimulus f_{AM}.

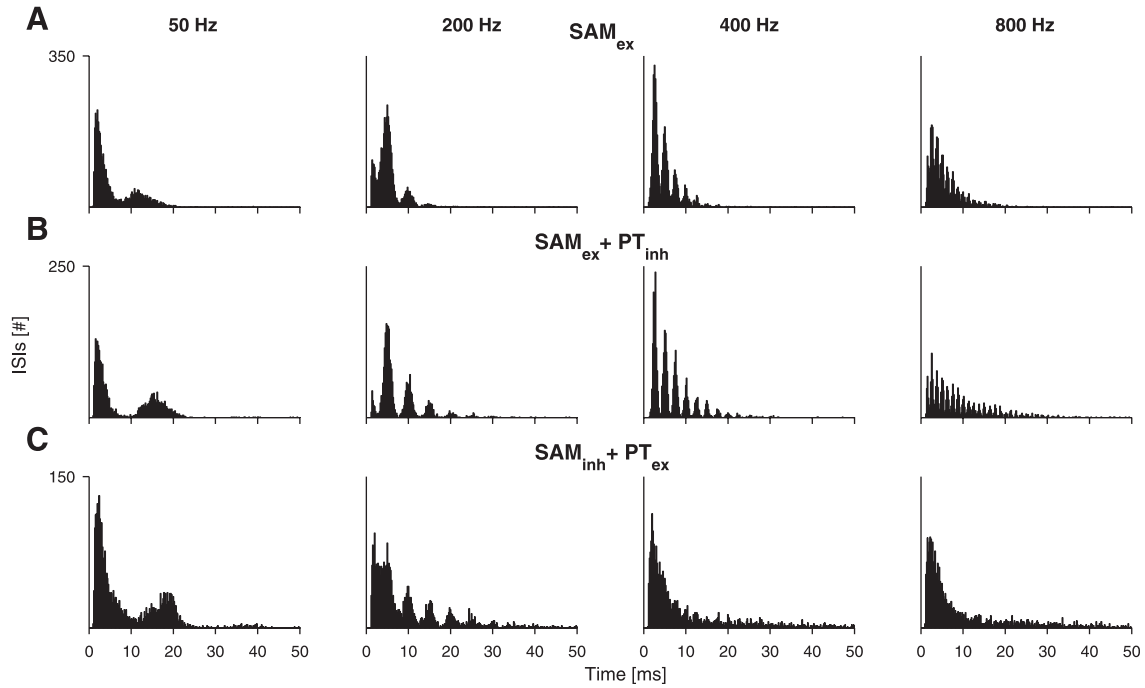

FIG. 5. Interspike interval (ISI) histograms for the responses to SAM signals (same unit as in Fig. 2). (A) ISI histograms of responses to SAM_{ex} stimulation for f_{AM} = 50, 200, 400 and 800 Hz. For f_{AM} = 50 Hz, note that the second ISI peak occurs at 12 ms and not at 20 ms as expected from the stimulus period. This might be due to the broad distribution of spikes over one stimulus period. (B) ISI for SAM_{ex} + PT_{inh}. The PT_{inh} is set at the center of the inhibitory sideband. Compared with A, the number of peaks at longer ISIs is increased, indicating an increment in skipping of stimulus cycles. Note that at f_{AM} = 50 Hz the second peak is shifted towards the actual stimulus period of 20 ms. (C) ISI histograms of responses to SAM_{inh} + PT_{ex} stimulation. At f_{AM} > 400 Hz the ISI histograms approach the form of an ISI histogram of pure tone stimulation, indicating the poorer following of the unit's response to the modulated tone.

Upon termination of the SAM_{inh} signal, the tonic response to the PT_{ex} is resumed. Note that response peaks occur anti-phasic to the SAM_{ex} condition (Fig. 3A), which can most clearly be seen in the period histograms (Fig. 6A and C).

In 34 units the whole range of f_{AM} could be covered for both SAM_{ex} and SAM_{inh} + PT_{ex} stimulation. To exclude effects of the SAM sidebands falling within the excitatory response areas, three units' responses to f_{AM} > 400 Hz were excluded from the analysis. The remaining 31 units had CFs between 1.6 and 33.6 kHz, and thresholds between 15 and 45 dB SPL. The units followed the SAM_{inh} + PT_{ex} stimulation showing a mean VS-MTF with band pass characteristic (Fig. 4, C1). The VS values of SAM_{ex} and SAM_{inh} + PT_{ex} differ significantly for $f_{AM} \geq 600$ Hz on the population level ($P < 0.01$, Mann–Whitney rank sum test) and for $f_{AM} \geq 400$ Hz on a cell-by-cell comparison ($P < 0.01$, Wilcoxon signed rank test, see Fig. 4, D1, gray dots). The maximum VS values were between 0.33 and 0.92 (0.71, SD 0.13) at f_{AM} between 20 and 600 Hz. At f_{AM} above optimum, VS values steadily decreased, but all units still followed the modulation up to 800 Hz. At 1000 Hz 27/31 units still had significant VS values.

Representative ISI histograms of one unit are shown in Fig. 5C. At f_{AM} of 50 and 200 Hz ISI histograms are comparable with ISI histograms of SAM_{ex}. At higher f_{AM} the individual peaks disappear, reflecting the lower VS values.

Modulation transfer properties – envelope reproduction

To distinguish between the two coding strategies, phase-locking and stimulus reproduction, we used the normalized correlation ($Corr_{norm}$) as a similarity measure between stimulus envelope and response PSTH (see Methods). Higher $Corr_{norm}$ values indicate more accurate reproduction of the stimulus shape by the firing rate, with a $Corr_{norm}$ value of one for perfect reproduction. In the following we describe the $Corr_{norm}$ values for all SAM conditions (same units as in the previous section) and relate them to the corresponding VS values.

SAM_{ex} condition

Normalized correlation values show an inverted band pass behaviour with respect to f_{AM} (Fig. 4, A2, 98 units, open circles, Friedman test $P << 0.001$). Smaller $Corr_{norm}$ values in the middle f_{AM} range (100–400 Hz) correspond to the band pass maximum of VS values (Fig. 4, A1). Similarly, for higher f_{AM} the fall-off observed in the VS values is accompanied by a sharp rise in $Corr_{norm}$ values to their maxima at f_{AM} 600–900 Hz.

SAM_{ex} + PT_{inh} vs. SAM_{ex}

The comparison of $Corr_{norm}$ values between SAM_{ex} and SAM_{ex} + PT_{inh} (Fig. 4, B2, open and filled circles, respectively) corresponds to the respective findings in VS values (Fig. 4, B1). At $f_{AM} \geq 500$ Hz $Corr_{norm}$ values show no significant difference between conditions, and nor do VS values. In the midrange (100–400 Hz), a comparison on a cell-by-cell level yielded significantly smaller $Corr_{norm}$ values for SAM_{ex} + PT_{inh} than $Corr_{norm}$ values for SAM_{ex} ($P < 0.01$, Wilcoxon signed rank test, Fig. 4, D2, black). Significant differences are also found for VS values in this f_{AM} range (Fig. 4, D1). However, for $f_{AM} \leq 50$ Hz the correspondence between $Corr_{norm}$ and VS with respect to the comparison of SAM_{ex} and SAM_{ex} + PT_{inh} ceases. While VS values differ significantly, no significant differences are present for $Corr_{norm}$ values (Fig. 4, D1 and

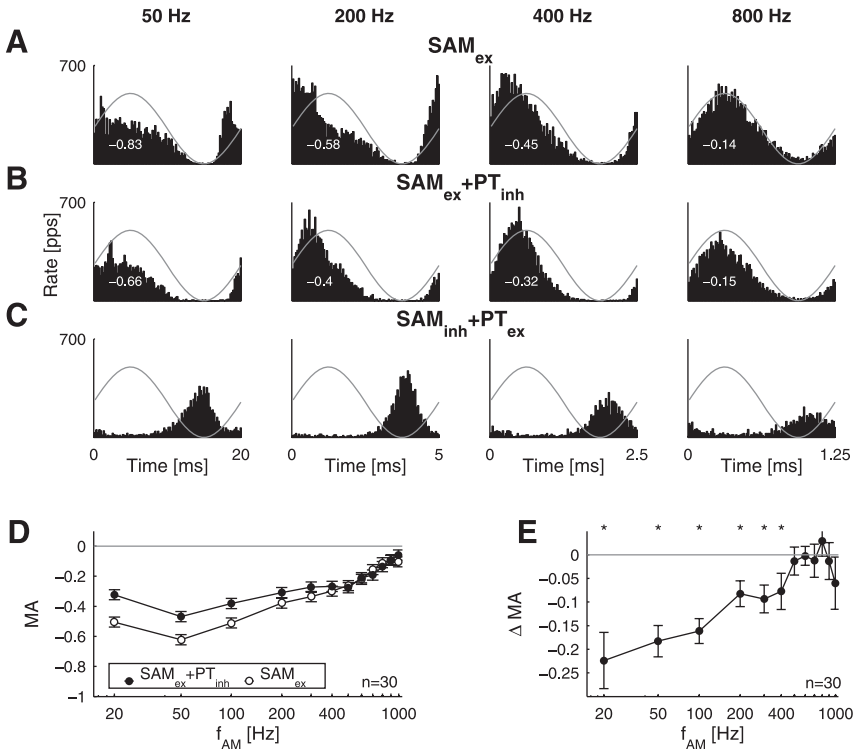

FIG. 6. Period histograms in response to SAM signals (G56807, CF 24.5 kHz, threshold 25 dB SPL) and comparison of symmetry of period histograms. (A) Period histograms of responses to SAM_{ex} stimulation. (B) Adding the PT_{inh} to SAM_{ex} stimulation causes the rising slopes of the period histogram to be less steep, i.e. rising and falling slopes become more symmetric. (C) Combining the PT_{ex} with SAM_{inh} causes shifts of the peaks of period histograms by half the period length, indicating that responses to the stimulus are maximal when the stimulus is lowest. Maximum asymmetry (MA) values for SAM_{ex} and SAM_{ex} + PT_{inh} stimulation are displayed in the bottom left corner of the respective period histograms. MA values for SAM_{inh} + PT_{ex} period histograms were not calculated, as the shape of the period histogram corresponds to the inverse of the inhibitory effect. (D) Absolute MA values of SAM_{ex} (open circles) and SAM_{ex} + PT_{inh} (filled circles) period histograms. The SAM_{ex} period histograms differ significantly from symmetry over the whole range of f_{AM}; the SAM_{ex} + PT_{inh} period histograms differ significantly from symmetry for $f_{AM} < 1000$ Hz ($P < 0.01$, Wilcoxon signed rank test). (E) Differences of the MA values of the period histograms between the SAM_{ex} and SAM_{ex} + PT_{inh} conditions are significant for $f_{AM} > 400$ Hz ($P < 0.01$, Wilcoxon signed rank test), indicating that in this range the onset response is prominently influenced by the pure tone inhibition. *$P < 0.01$.

D2, respectively). This finding originates in the property of $Corr_{norm}$ to quantify the distance from the stimulus envelope. Thus, a response that is less phase-precise than the stimulus (SAM_{ex} f_{AM} = 20 Hz: VS < 0.5, Fig. 4, B1, open symbol) changes to a response that is more phase-precise than the stimulus (SAM_{ex} + PT_{inh} f_{AM} = 20 Hz: VS > 0.5, Fig. 4, B1, filled symbol). In this situation the distances to the stimulus envelope do not differ significantly: the former is too broad and the latter too peaked to reproduce the stimulus envelope.

SAM_{inh} + PT_{ex} vs. SAM_{ex}

Although $Corr_{norm}$ values tend to be lower for SAM_{inh} + PT_{ex} than for SAM_{ex} at $f_{AM} \leq 100$ Hz (Fig. 4, C2, gray and open circles, respectively), they do not differ significantly at the $P = 0.01$ level (minimal $P = 0.06$ at $f_{AM} = 50$ Hz). Likewise, VS values show no significant difference in this f_{AM} range (Fig. 4, C1). At $f_{AM} > 100$ Hz $Corr_{norm}$ values for SAM_{inh} + PT_{ex} increase. This increase is paralleled by a sharp reduction of VS values. $Corr_{norm}$ values start to decrease at $f_{AM} \geq 600$ Hz, the f_{AM} value when the VS values for SAM_{inh} + PT_{ex} stimulation reach 0.5. $Corr_{norm}$ values for the SAM_{inh} + PT_{ex} condition are significantly different to the SAM_{ex} condition at $f_{AM} = 1000$ Hz ($P < 0.01$, Mann–Whitney rank sum test).

In summary, the changes in $Corr_{norm}$ values with increasing f_{AM} take a mostly opposite course to the respective VS values. This is to be expected, given the trade-off between phase-locking and the reproduction of the stimulus envelope, i.e. a perfectly phase-locked response cannot reproduce the stimulus well and vice versa. Interestingly, responses with VS values close to VS of the stimulus envelope ($VS_{SAM} = 0.5$) did correspond to the highest $Corr_{norm}$ values, a correspondence that does not reflect an intrinsic coupling between the measures (see Methods). Hence, in the present data set VS values of 0.5 generally indicated envelope reproduction. Only in the case of SAM_{inh} + PT_{ex}, does coding of both envelope and phase-locking seem to degrade at higher f_{AM}.

Latencies of excitation and inhibition

Dynamic integration of rate-increasing and rate-decreasing stimuli depends on the modulation properties and latency of the responses. Both measures of response modulation, VS and $Corr_{norm}$ values, were quantified independently of the response latency. Therefore, we next estimated the onset and ongoing latencies of rate-increasing and rate-decreasing stimuli.

Excitatory response latency: onset vs. ongoing

To compare the onset (HA) to the ongoing (PCC) latencies both measures were computed for 100 units for which more than one

SAM stimulation for $f_{AM} \geq 600$ Hz had been tested. The average ongoing latency based on the PCC method was 3.47 ms (SD 0.55), whereas the HA method led to an average onset latency of 3.9 ms (SD 1.1). Surprisingly, the correlation between the two latencies was quite weak ($r = 0.28$) (Fig. 7A, all circles). This lack of correlation can derive from multiple sources: (1) the two methods could estimate two different aspects of latency or (2) the standard deviation of one or both methods is so large that the correlation is hidden. To distinguish between these possibilities, we singled out the latencies obtained from stimulations ≥ 35 dB above CF threshold (Fig. 7A, black circles), where the spread in the onset latency measure has dropped significantly (Fig. 2C). The correlation between the two latencies then increases to $r = 0.91$ with a mean difference $\Delta(t_{PCC}-t_{HA}) = 0.6$ ms (SD 0.37). Consequently, the lack of correlation for the total data set must be due to the significantly increased spread of the onset latency for levels close to threshold. Note that in general, a spread of latencies is to be expected for any method as (1) the tonotopic propagation latencies along the basilar membrane in the cochlea are conveyed to the MNTB (high- to low-frequency delay difference in the cochlea; Schmiedt & Zwislocki, 1977, figs 19 and 21) and (2) latencies of different MNTB cells will differ intrinsically.

Influence of inhibition on ongoing latencies

The mean excitatory ongoing latency for SAM_{ex} was 3.39 ms (SD 0.43) and increased to an average of 3.50 ms (SD 0.47) when the PT_{inh} was added (Fig. 7B, 30 units). This corresponds to an average increase of 0.11 ms (SD 0.14), which was significantly greater than 0 ($P < 0.001$, Wilcoxon signed rank test). The correlation coefficient between the two conditions is very high ($r = 0.95$) indicating that these results are consistent across cells. The most likely explanation for this increase in excitatory ongoing latency is tonic inhibition delaying the response slightly. Another possible explanation is that the onset components are more pronounced in the SAM_{ex} condition, which would shift the ongoing latencies to lower values. However, this explanation can be rejected, as we computed ongoing latencies only based on $f_{AM} \geq 600$ Hz, where the MA values of the responses already ceased to be significantly different between the conditions SAM_{ex} and $SAM_{ex} + PT_{inh}$ (Fig. 6E).

Ongoing latencies: excitation vs. inhibition

Next, we compared excitatory and inhibitory ongoing latencies using the PCC method for responses to SAM_{ex} and $SAM_{inh} + PT_{ex}$ stimulation ($n = 31$, multiple recordings with $f_{AM} \geq 600$ Hz for both conditions, see above). The average excitatory ongoing latency was 3.40 ms (SD 0.47) and thus shorter than the average inhibitory ongoing latency of 3.59 ms (SD 0.47) (Fig. 7C, filled circles). On the basis of a cell-by-cell comparison, inhibition was delayed with respect to excitation by 0.18 ms (SD 0.31). This difference was significantly > 0 ($P < 0.003$, Wilcoxon signed rank test). In summary, a high degree of correlation exists between excitatory and inhibitory response latencies on the level of individual cells (evidenced by the correlation coefficient: $r = 0.78$, $P < 10^{-6}$), with inhibition following excitation at a submillisecond difference.

Onset latencies: excitation vs. inhibition

Measurements of the onset latencies based on HA/HR readings were based on two-tone PSTHs (20 units, 150 repetitions, for detailed description of acquisition see Kopp-Scheinpflug *et al.*, 2003b). The levels for the excitatory and the inhibitory stimuli were matched by choosing the same dB-distance to threshold at the respective frequencies. The HA/HR comparison shows excitation preceding inhibition by 1.46 ms (SD 1.16) ($P < 0.001$, Wilcoxon signed rank test), yet the relationship between the two conditions is more variable than for the respective measurements of ongoing latencies. If the same absolute stimulus level had been chosen for the excitatory and the inhibitory stimulus, even smaller values would have been obtained for excitatory onset latencies, thus arriving at the same qualitative results (results not shown). A likely interpretation for the different relative onset latencies is that the onset dynamics of inhibition are slower than the onset dynamics of excitation. This is in line with results from tone burst stimulations at frequencies at the transition from the excitatory to the inhibitory response area. Such stimuli cause a pronounced onset

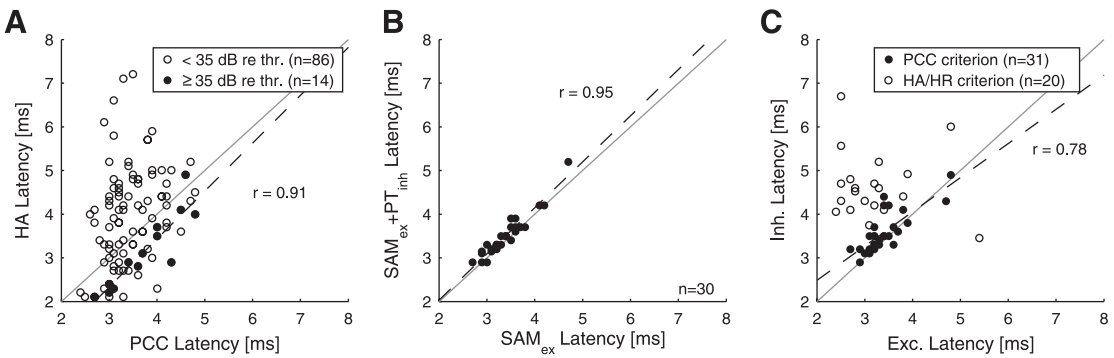

FIG. 7. Comparison of response latencies under various conditions. (A) Cell-by-cell comparison of onset and ongoing latencies. The lack of correlation between the two measures (all circles; $r = 0.28$) is due to the variability in onset latency. When only the stimulus levels exceeding the threshold by more than 35 dB (filled circles) are considered, the correlation between the two measures becomes highly significant ($r = 0.91$, dashed line). (B) Cell-by-cell comparison of ongoing latencies under the SAM_{ex} and $SAM_{ex} + PT_{inh}$ conditions; the latter leads by 0.11 ms (SD 0.14) over the former ($P < 0.001$, Wilcoxon signed rank test, $r = 0.95$, dashed line). (C) Cell-by-cell comparison of ongoing latencies of excitation and inhibition (filled circles, based on SAM_{ex} and $SAM_{inh} + PT_{ex}$ data) and onset latencies of excitation and inhibition (open circles, based on two-tone PSTH data). During SAM stimulation ongoing latencies of excitation and inhibition are close with excitation leading by 0.18 ms (SD 0.31) ($P < 0.005$, Wilcoxon signed rank test, $r = 0.78$, dashed line). Onset latencies of excitation are shorter than onset latencies of inhibition [1.46 ms (SD 1.16), $P < 0.001$, Wilcoxon signed rank test].

peak followed by no or only sparse firing for the duration of the tone (data not shown).

Discussion

The present study shows that MNTB units in the gerbil are able to encode rapid envelope fluctuations in their time-varying firing rate, thereby establishing a precisely timed inhibitory input to the nucleus' projection targets. Remarkably, excitatory and inhibitory rate changes showed similar temporal fidelity in modulating the MNTB firing rate. The relative timing of excitatory and inhibitory rate changes was shown to be close, with inhibition following excitation on average by just 0.2 ms.

Coding of temporal properties of the stimulus

For the downstream processing in their target nuclei the MNTB principal cells must convey all the required information, e.g. for the on/offset of stimuli the stimulus level, dynamically altered stimulus levels and – for low frequencies – the phase of the input signal. Here, we compared how well two different coding strategies – phase-locking and envelope reproduction – describe the response of MNTB neurons to amplitude modulations. The results indicate that both strategies, i.e. the extraction of temporal information and rate-coded reproduction of the instantaneous stimulus intensity, are realized to different degrees. Determinants are the f_{AM} of the afferent signal and whether a carrier eliciting excitation or inhibition was used.

SAM_{ex} vs. SAM_{inh} phase-locking

Phase-locking occurs for both excitatory and inhibitory SAM, as indicated by VS values exceeding the SAM-associated VS value of 0.5, with the fidelity of responses varying with f_{AM}. A considerable percentage of units (35%) phase-locked to excitatory signals even at f_{AM} as high as 1000 Hz. This corresponds to previous *in vitro* and *in vivo* studies. Electric pulse-train stimulation in brain slices induced faithful responses even at frequencies > 600 Hz (Wu & Kelly, 1993; Taschenberger & von Gersdorff, 2000). Also, phase-locked responses to SAM signals were shown in *in vivo* MNTB preparations in cats and mice (Joris & Yin, 1998; Kopp-Scheinpflug *et al.*, 2003a). Presently, in 10% of cells phase-locked responses to inhibitory f_{AM} signals were observed up to 1000 Hz. Like the excitatory VS-MTFs, inhibitory VS-MTFs featured low pass or band pass characteristics and showed maximum phase-locking between 20 and 600 Hz. The only other study investigating responses to inhibitory and excitatory AM signals in the auditory brainstem *in vivo* yielded similar results: Moller (1975a) reported comparable shapes of VS-MTFs in cochlear nucleus neurons. More recently, Li *et al.* (2006) have shown similar results in the inferior colliculus.

SAM_{ex}: phase-locking vs. envelope encoding

When comparing VS and $Corr_{norm}$ values of SAM_{ex} stimulation, it becomes evident that phase-locking to the stimulus outweighs stimulus envelope reproduction at moderate f_{AM} (100–500 Hz). The reverse is observed at higher f_{AM} (≥ 600 Hz); the units' firing reproduces the stimulus envelope rather than phase-locking to it. At lower f_{AM} (< 100 Hz), both coding strategies are realized in MNTB units. The relationship between the onset and the tonic component of the units' discharge activity plays an important role in this frequency dependency: at low f_{AM}, the response onset causes moderate VS values, while the tonic component leads to high $Corr_{norm}$ values. At moderate f_{AM}, the shortened tonic component facilitates high VS values and prevents high $Corr_{norm}$ values, i.e. phase-locking dominates over stimulus reproduction. In the case of high f_{AM}, the responses are mostly made up of brief, onset-like components, the shapes of which match one period of the sinusoidal envelope leading to high $Corr_{norm}$ values and low VS values. It should be noted that using SAM rather than random AM suffers from a caveat: a constant amount of Gaussian spike time jitter can broaden a phase-locked response (Paolini *et al.*, 2001), which will be most severe at high f_{AM}. This could lead to a similar profile as that of the *sinusoidal* AM itself. If this is the case, it could explain the high $Corr_{norm}$ values for high f_{AM}.

SAM_{inh}: phase-locking vs. envelope encoding

Responses to SAM_{inh} are similar to SAM_{ex} stimulation up to moderate f_{AM}; phase-locking to the stimulus is associated with a poor reproduction of the stimulus envelope and vice versa. However, in the case of high f_{AM} this generalization does not apply. In the majority of units VS and $Corr_{norm}$ approach values observed in unmodulated responses. Apparently, the efficiency of inhibition in modulating the units' responses at high f_{AM} is restricted to a small set of units.

Implications for target nuclei of the MNTB

The major target nucleus of the MNTB, the LSO, which encodes azimuthal sound location based on interaural intensity differences, relies on afferents accurately encoding AM in the acoustic stimulus (for reviews see Yin, 2002; Tollin, 2003). Here, we show that the preservation of AM is not only realized in the excitatory response areas of MNTB units, but extends further to the inhibitory response areas possibly influencing the sensitivity to interaural intensity differences in LSO neurons.

Furthermore, inhibitory projections from the MNTB are crucial for computing sound locations on the basis of interaural time differences in the MSO (Brand *et al.*, 2002; Zhou *et al.*, 2005). As these interaural time differences are computed from phase-locked responses to low-frequency tones rather than to envelope modulations, the present results do not apply crucially to the evaluation of the processing in the MSO. Still, the inhibitory projections from the MNTB might influence high-CF neurons in the MSO, which were shown to be sensitive to interaural time differences between envelope modulations in ipsilateral and contralateral acoustic stimuli (Joris, 1996; Batra *et al.*, 1997). As these high-frequency MSO neurons project to the inferior colliculus, MNTB response properties will also influence AM processing in this midbrain nucleus (Yin *et al.*, 1984; Batra *et al.*, 1989, 1993).

From the pharmacological manipulation of neurons of the superior paraolivary nucleus it was concluded that inhibitory projections from the MNTB are essential for establishing off-responses in its principal neurons (Kulesza *et al.*, 2007). The present results are consistent with this idea: the frequency range of AM which causes off-responses in units of the superior paraolivary nucleus (< 1000 Hz, Kuwada & Batra, 1999; = 400 Hz, Kulesza *et al.*, 2003) is compatible with the phase-locking range in MNTB units (≤ 1000 Hz, present study). Similarly, phase-locking to inhibitory AM in MNTB units would also lead to phase-locked responses in units of the superior paraolivary nucleus.

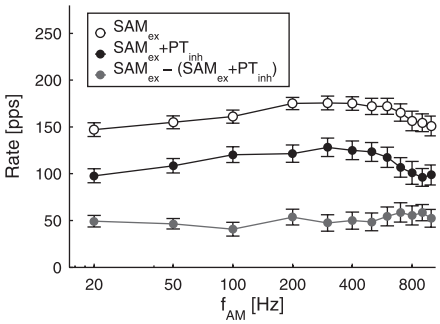

FIG. 8. Average discharge rates in response to SAM_{ex} and SAM_{ex} + PT_{inh} stimulation. The discharge rate to the SAM_{ex} stimulus (open black circles) is markedly reduced when the PT_{inh} is added (filled black circles). The amount of reduction (51 pps, SD 5 pps) is almost independent of f_{AM} (filled dark gray circles). Additionally, results of a simulation are shown (open light gray squares), which predicts the rate-reduction based on the assumption that an inhibition-induced time- and stimulus-independent rate reduction causes the observed increase in VS values. The data differ markedly from the simulation by not showing a decrease in VS values for higher f_{AM}, which indicates the effect of a time- or stimulus-dependent inhibition. The simulation consisted simply of estimating the required rate reduction (i.e. subtraction of a constant rate) of the SAM_{ex} period histogram during the SAM_{ex} to attain the observed VS value from the SAM_{ex} + PT_{inh} condition. To this end a program was custom written (based on *fminsearch* in MATLAB) where the difference in VS values served as the minimization criterion. If negative discharge rates occurred during minimization they were set to 0.

Interaction of different frequencies can improve phase-locking

The present study shows that spectral energy placed within the center of the inhibitory sidebands of MNTB units increases their ability to phase-lock to f_{AM} up to 600 Hz. The underlying mechanism seems to be related to the almost constant reduction of acoustically evoked discharge rates occurring over the whole range of f_{AM} (Fig. 8). Other studies have found a similar effect on the phase-locking ability in different nuclei, when discharge rates were reduced by pharmacological manipulation (Backoff *et al.*, 1999) or by adding background noise (Rees & Moller, 1987; Rees & Palmer, 1989; Frisina *et al.*, 1994, 1996). Usually reduction in discharge rate led to increases in phase-locking (but see also Behrend *et al.*, 2002).

As has been suggested previously (e.g. Frisina *et al.*, 1994), this increase in phase-locking through sideband stimulation could be beneficial in situations of ambient noise. Without sideband inhibition, noise would reduce the range of responsiveness to amplitude changes, degrading the neuron's ability to encode AM. Sideband inhibition could serve to move the modulatory range to the ambient level.

Relative timing of excitation and inhibition

The relative timing of excitatory and inhibitory rate changes can qualitatively be described as inhibition immediately following excitation. Yet, on a quantitative level, the timing is determined by the stimulus history, as indicated by the different results of onset and ongoing latency measures. If a given stimulus, eliciting a combined excitatory/inhibitory response, follows a period of subthreshold stimuli, then the inhibitory response is delayed with respect to the excitatory response by more than a millisecond (HA/HR measure). If, however, an ongoing stimulation is considered, then the inhibitory response is delayed by only a fraction of a millisecond (PCC measure).

The dependence of the relative timing of excitation and inhibition on the stimulus history influences stimulus processing differently. At stimulus onset, the first few spikes are triggered without an inhibitory impact. After a few milliseconds, inhibition has built up sufficiently to gate or fully suppress spiking. During ongoing stimulation, however, inhibitory and excitatory ongoing latencies are so close that inhibition immediately interacts with excitation and effectively reduces spike activity. This is in line with theories of neuronal processing, where the first spikes are hypothesized to provide an initial sketch of a specific stimulus and the subsequent response filling in more refined details (Thorpe *et al.*, 2001).

Source of inhibition

The stimulus-induced reductions in discharge rates could be caused by different mechanisms, either cochlear suppression, neuronal inhibition or a mixture of both. As the frequency–intensity profiles of inhibitory and suppressive sidebands can be very similar, the contribution of either mechanism cannot easily be distinguished.

Unlike neuronal inhibition, cochlear two-tone suppression (CTTS) is not based on neuronal connections, but stems from active processes mediated by the outer hair cells (Pickles, 1988; Ruggero *et al.*, 1992). Therefore, CTTS can already be demonstrated on the basilar membrane (Ruggero *et al.*, 1992) and in auditory nerve fibers (Delgutte, 1990), and should be recoverable on subsequent stages of the auditory pathway as well. The observed correlation of excitatory and inhibitory response latencies, the PSTH shape and the position of the inhibitory sidebands would be compatible with known properties of CTTS (Sachs & Kiang, 1968; Arthur *et al.*, 1971; Sellick & Russell, 1979; Ruggero *et al.*, 1992; for reviews see Pickles, 1988; Robles & Ruggero, 2001).

CTTS and neuronal inhibition can possibly be distinguished by their ability to suppress the spontaneous activity of inner hair cells/auditory nerve fibers. The currently dominant view (Pickles, 1988) is that cochlear suppression does not reduce spontaneous firing. This is in contrast to some earlier studies, which showed pronounced and long-lasting reductions in spontaneous firing following the presentation of single off-CF tones (Katsuki *et al.*, 1961; Rupert *et al.*, 1963; Sachs & Kiang, 1968; Henry & Lewis, 1992). Other studies, however, did not show such reduced spontaneous activity (Kiang *et al.*, 1965; Hind *et al.*, 1967). If the currently dominant view proves to be correct, i.e. no reduction of spontaneous rate due to single tones, then it is doubtful that CTTS is the sole source of the rate reduction observed here, as inhibitory sidebands were observed in about 60% of spontaneously active MNTB units (f_{spont} > 30 Hz) during the presentation of single tones at various frequencies and intensities.

Neuronal inhibition is likely to contribute to signal processing. It could either be already introduced at the level of the cochlear nucleus or directly in the MNTB, as inhibitory terminals are known to terminate both on globular bushy cells and on MNTB principal cells (Martin & Dickson, 1983; Roberts & Ribak, 1987; Wenthold *et al.*, 1987; Adams & Mugnaini, 1990; Benson & Potashner, 1990; Juiz *et al.*, 1996; Ostapoff *et al.*, 1997; Spirou *et al.*, 2005). In globular bushy cells, inhibitory response areas were shown to be organized in sidebands similar to those observed in MNTB units (Brownell, 1975; Martin & Dickson, 1983; Spirou *et al.*, 1990; Rhode & Greenberg, 1994b). Thus, the calyx might simply convey rate reductions launched at globular bushy cells. Still, neuronal inhibition could additionally contribute to these rate reductions at the level of the MNTB. In *in vitro* physiological studies both glycine and GABA were shown to affect MNTB principal cells (Banks & Smith, 1992; Wu & Kelly, 1995; Turecek & Trussell, 2001; Awatramani *et al.*, 2004, 2005). Based on a comparison of

the effective time-constants of GABA (∼5 ms, Awatramani *et al.*, 2005) and glycine (∼1.1 ms, Awatramani *et al.*, 2004) required for following high-frequency AM inhibitory stimuli, only the rapid action of glycine is compatible with significant VS values at 1000 Hz modulation and with the gradual decrease of VS values above ∼300 Hz.

Although the origin of the observed rate reductions still needs further investigation, the present study shows that such rate reductions are similarly well represented in the MNTB to rate increases. In particular, the temporal coding of dynamic stimuli benefits from the integration across frequency channels. Thus, the MNTB can provide a temporally precise inhibitory input to the processing in the auditory brainstem across a wide range of frequencies.

Acknowledgements

We are grateful for the support of G. Dobof who pointed us to some crucial aspects of the data's implications. This work was supported by the Deutsche Forschungsgemeinschaft (Ru 390–18/1). B.E. and S.T. acknowledge support from the Graduate Program INTERNEURO (DFG GRK 1097) at the University of Leipzig.

Abbreviations

AM, amplitude modulation; CF, characteristic frequency; $Corr_{norm}$, normalized correlation between stimulus envelope and unit's response; CTTS, cochlear two-tone suppression; f_{AM}, modulation frequency; HA/HR, half-maximum activation/reduction; ISI, interspike interval; LSO, lateral superior olive; MA, maximum asymmetry; MNTB, medial nucleus of the trapezoid body; MSO, medial superior olive; MTF, modulation transfer function; PCC, periodic cross correlation; PSTH, post-stimulus time histogram; SAM, sinusoidal amplitude modulation; $SAM_{ex} + PT_{inh}$, SAM stimulation at the unit's CF and pure tone stimulation within the unit's inhibitory response area; SAM_{ex}, SAM stimulation at the unit's CF; $SAM_{inh} + PT_{ex}$, SAM stimulation within the unit's inhibitory response area and pure tone stimulation at the unit's CF; VS, vector strength.

References

Adams, J.C. (1981) Heavy metal intensification of DAB-based product. *J. Histochem. Cytochem.*, **29**, 775.

Adams, J.C. & Mugnaini, E. (1990) Immunocytochemical evidence for inhibitory and disinhibitory circuits in the superior olive. *Hear. Res.*, **49**, 281–298.

Arthur, R.M., Pfeiffer, R.R. & Suga, N. (1971) Properties of 'two-tone inhibition' in primary auditory neurones. *J. Physiol.*, **212**, 593–609.

Awatramani, G.B., Turecek, R. & Trussell, L.O. (2004) Inhibitory control at a synaptic relay. *J. Neurosci.*, **24**, 2643–2647.

Awatramani, G.B., Turecek, R. & Trussell, L.O. (2005) Staggered development of GABAergic and glycinergic transmission in the MNTB. *J. Neurophysiol.*, **93**, 819–828.

Backoff, P.M., Shadduck Palombi, P. & Caspary, D.M. (1999) Gamma-aminobutyric acidergic and glycinergic inputs shape coding of amplitude modulation in the chinchilla cochlear nucleus. *Hear. Res.*, **134**, 77–88.

Banks, M.I. & Smith, P.H. (1992) Intracellular recordings from neurobiotin-labeled cells in brain slices of the rat medial nucleus of the trapezoid body. *J. Neurosci.*, **12**, 2819–2837.

Batra, R., Kuwada, S. & Stanford, T.R. (1989) Temporal coding of envelopes and their interaural delays in the inferior colliculus of the unanesthetized rabbit. *J. Neurophysiol.*, **61**, 257–268.

Batra, R., Kuwada, S. & Stanford, T.R. (1993) High-frequency neurons in the inferior colliculus that are sensitive to interaural delays of amplitude-modulated tones: evidence for dual binaural influences. *J. Neurophysiol.*, **70**, 64–80.

Batra, R., Kuwada, S. & Fitzpatrick, D.C. (1997) Sensitivity to interaural temporal disparities of low- and high-frequency neurons in the superior olivary complex. I. Heterogeneity of responses. *J. Neurophysiol.*, **78**, 1222–1236.

Behrend, O., Brand, A., Kapfer, C. & Grothe, B. (2002) Auditory response properties in the superior paraolivary nucleus of the gerbil. *J. Neurophysiol.*, **87**, 2915–2928.

Benson, C.G. & Potashner, S.J. (1990) Retrograde transport of [3H]glycine from the cochlear nucleus to the superior olive in the guinea pig. *J. Comp. Neurol.*, **296**, 415–426.

Brand, A., Behrend, O., Marquardt, T., McAlpine, D. & Grothe, B. (2002) Precise inhibition is essential for microsecond interaural time difference coding. *Nature*, **417**, 543–547.

Brownell, W.E. (1975) Organization of the cat trapezoid body and the discharge characteristics of its fibers. *Brain Res.*, **94**, 413–433.

Delgutte, B. (1990) Two-tone rate suppression in auditory-nerve fibers: dependence on suppressor frequency and level. *Hear. Res.*, **49**, 225–246.

Frisina, R.D., Walton, J.P. & Karcich, K.J. (1994) Dorsal cochlear nucleus single neurons can enhance temporal processing capabilities in background noise. *Exp. Brain Res.*, **102**, 160–164.

Frisina, R.D., Karcich, K.J., Tracy, T.C., Sullivan, D.M., Walton, J.P. & Colombo, J. (1996) Preservation of amplitude modulation coding in the presence of background noise by chinchilla auditory-nerve fibers. *J. Acoust. Soc. Am.*, **99**, 475–490.

Glendenning, K.K., Brunso-Bechtold, J.K., Thompson, G.C. & Masterton, R.B. (1981) Ascending auditory afferents to the nuclei of the lateral lemniscus. *J. Comp. Neurol.*, **197**, 673–703.

Goldberg, J.M. & Brown, P.B. (1969) Response of binaural neurons of dog superior olivary complex to dichotic tonal stimuli: some physiological mechanisms of sound localization. *J. Neurophysiol.*, **32**, 613–636.

Greenwood, J.A. & Durand, D. (1955) The distribution of length and components of the sum of n random unit vectors. *Annals Math. Statist.*, **26**, 233–246.

Guinan, J.J. Jr & Li, R.Y. (1990) Signal processing in brainstem auditory neurons which receive giant endings (calyces of Held) in the medial nucleus of the trapezoid body of the cat. *Hear. Res.*, **49**, 321–334.

Guinan, J.J. Jr, Guinan, S.S. & Norris, B.E. (1972a) Single auditory units in the superior olivary complex I: responses to sounds and classification based on physiological properties. *Int. J. Neurosci.*, **4**, 101–120.

Guinan, J.J. Jr, Norris, B.E. & Guinan, S.S. (1972b) Single auditory units in the superior olivary complex II: locations of unit categories and tonotopic organization. *Int. J. Neurosci.*, **4**, 147–166.

Henry, K.R. & Lewis, E.R. (1992) One-tone suppression in the cochlear nerve of the gerbil. *Hear. Res.*, **63**, 1–6.

Hind, J.E., Anderson, D.J., Brugge, J.F. & Rose, J.E. (1967) Coding of information pertaining to paired low-frequency tones in single auditory nerve fibers of the squirrel monkey. *J. Neurophysiol.*, **30**, 794–816.

Joris, P.X. (1996) Envelope coding in the lateral superior olive. II. Characteristic delays and comparison with responses in the medial superior olive. *J. Neurophysiol.*, **76**, 2137–2156.

Joris, P.X. & Yin, T.C. (1992) Responses to amplitude-modulated tones in the auditory nerve of the cat. *J. Acoust. Soc. Am.*, **91**, 215–232.

Joris, P.X. & Yin, T.C.T. (1998) Envelope coding in the lateral superior olive. III. Comparison with afferent pathways. *J. Neurophysiol.*, **79**, 253–269.

Juiz, J.M., Helfert, R.H., Bonneau, J.M., Wenthold, R.J. & Altschuler, R.A. (1996) Three classes of inhibitory amino acid terminals in the cochlear nucleus of the guinea pig. *J. Comp. Neurol.*, **373**, 11–26.

Kass, R.E., Ventura, V. & Brown, E.N. (2005) Statistical issues in the analysis of neuronal data. *J. Neurophysiol.*, **94**, 8–25.

Katsuki, Y., Kanno, Y., Suga, N. & Mannen, M. (1961) Primary auditory neurons of monkey. *Jpn. J. Physiol.*, **11**, 678–683.

Kiang, N.Y., Watanabe, T., Thomas, E.C. & Clark, L.F. 1965. *Discharge Patterns of Single Fibers in the Cat's Auditory Nerve*. The MIT Press, Cambridge, Mass.

Knipschild, M., Dorrscheidt, G.J. & Rubsamen, R. (1992) Setting complex tasks to single units in the avian auditory forebrain. I: Processing of complex artificial stimuli. *Hear. Res.*, **57**, 216–230.

Kopp-Scheinpflug, C., Dehmel, S., Dorrscheidt, G.J. & Rubsamen, R. (2002) Interaction of excitation and inhibition in anteroventral cochlear nucleus neurons that receive large endbulb synaptic endings. *J. Neurosci.*, **22**, 11004–11018.

Kopp-Scheinpflug, C., Fuchs, K., Lippe, W.R., Tempel, B.L. & Rubsamen, R. (2003a) Decreased temporal precision of auditory signaling in Kcna1-null mice: an electrophysiological study in vivo. *J. Neurosci.*, **23**, 9199–9207.

Kopp-Scheinpflug, C., Lippe, W.R., Dorrscheidt, G.J. & Rubsamen, R. (2003b) The medial nucleus of the trapezoid body in the gerbil is more than a relay: comparison of pre- and postsynaptic activity. *J. Assoc. Res. Otolaryngol.*, **4**, 1–23.

Kulesza, R.J. Jr, Spirou, G.A. & Berrebi, A.S. (2003) Physiological response properties of neurons in the superior paraolivary nucleus of the rat. *J. Neurophysiol.*, **89**, 2299–2312.

Kulesza, R.J. Jr, Kadner, A. & Berrebi, A.S. (2007) Distinct roles for glycine and GABA in shaping the response properties of neurons in the superior paraolivary nucleus of the rat. *J. Neurophysiol.*, **97**, 1610–1620.
Kuwabara, N. & Zook, J.M. (1991) Classification of the principal cells of the medial nucleus of the trapezoid body. *J. Comp. Neurol.*, **314**, 707–720.
Kuwabara, N., DiCaprio, R.A. & Zook, J.M. (1991) Afferents to the medial nucleus of the trapezoid body and their collateral projections. *J. Comp. Neurol.*, **314**, 684–706.
Kuwada, S. & Batra, R. (1999) Coding of sound envelopes by inhibitory rebound in neurons of the superior olivary complex in the unanesthetized rabbit. *J. Neurosci.*, **19**, 2273–2287.
Li, H., Sabes, J.H. & Sinex, D.G. (2006) Responses of inferior colliculus neurons to SAM tones located in inhibitory response areas. *Hear. Res.*, **220**, 116–125.
Martin, M.R. & Dickson, J.W. (1983) Lateral inhibition in the anteroventral cochlear nucleus of the cat: a microiontophoretic study. *Hear. Res.*, **9**, 35–41.
Moller, A.R. (1975a) Dynamic properties of excitation and inhibition in the cochlear nucleus. *Acta Physiol. Scand.*, **93**, 442–454.
Moller, A.R. (1975b) Latency of unit responses in cochlear nucleus determined in two different ways. *J. Neurophysiol.*, **38**, 812–821.
Moller, A.R. (1976) Dynamic properties of excitation and two-tone inhibition in the cochlear nucleus studied using amplitude-modulated tones. *Exp. Brain Res.*, **25**, 307–321.
Ostapoff, E.M., Benson, C.G. & Saint Marie, R.L. (1997) GABA- and glycine-immunoreactive projections from the superior olivary complex to the cochlear nucleus in guinea pig. *J. Comp. Neurol.*, **381**, 500–512.
Paolini, A.G., Fitzgerald, J.V., Burkitt, A.N. & Clark, G.M. (2001) Temporal processing from the auditory nerve to the medial nucleus of the trapezoid body in the rat. *Hear Res.*, **159**, 101–116.
Pickles, J.O. 1988. *An Introduction to the Physiology of Hearing*. Academic Press Limited, New York.
Rees, A. & Moller, A.R. (1987) Stimulus properties influencing the responses of inferior colliculus neurons to amplitude-modulated sounds. *Hear. Res.*, **27**, 129–143.
Rees, A. & Palmer, A.R. (1989) Neuronal responses to amplitude-modulated and pure-tone stimuli in the guinea pig inferior colliculus, and their modification by broadband noise. *J. Acoust. Soc. Am.*, **85**, 1978–1994.
Rhode, W.S. & Greenberg, S. (1994a) Encoding of amplitude modulation in the cochlear nucleus of the cat. *J. Neurophysiol.*, **71**, 1797–1825.
Rhode, W.S. & Greenberg, S. (1994b) Lateral suppression and inhibition in the cochlear nucleus of the cat. *J. Neurophysiol.*, **71**, 493–514.
Roberts, R.C. & Ribak, C.E. (1987) GABAergic neurons and axon terminals in the brainstem auditory nuclei of the gerbil. *J. Comp. Neurol.*, **258**, 267–280.
Robles, L. & Ruggero, M.A. (2001) Mechanics of the mammalian cochlea. *Physiol. Rev.*, **81**, 1305–1352.
Ruggero, M.A., Robles, L. & Rich, N.C. (1992) Two-tone suppression in the basilar membrane of the cochlea: mechanical basis of auditory-nerve rate suppression. *J. Neurophysiol.*, **68**, 1087–1099.
Rupert, A., Moushegian, G. & Galambos, R. (1963) Unit responses to sound from auditory nerve of the cat. *J. Neurophysiol.*, **26**, 449–465.
Sachs, M.B. & Kiang, N.Y. (1968) Two-tone inhibition in auditory-nerve fibers. *J. Acoust. Soc. Am.*, **43**, 1120–1128.
Schmiedt, R.A. & Zwislocki, J.J. (1977) Comparison of sound-transmission and cochlear-microphonic characteristics in Mongolian gerbil and guinea pig. *J. Acoust. Soc. Am.*, **61**, 133–149.
Sellick, P.M. & Russell, I.J. (1979) Two tones suppression in the cochlear hair cells. *Hear. Res.*, **1**, 227–236.
Smith, P.H. & Rhode, W.S. (1987) Characterization of HRP-labeled globular bushy cells in the cat anteroventral cochlear nucleus. *J. Comp. Neurol.*, **266**, 360–375.
Smith, P.H., Joris, P.X. & Yin, T.C. (1998) Anatomy and physiology of principal cells of the medial nucleus of the trapezoid body (MNTB) of the cat. *J. Neurophysiol.*, **79**, 3127–3142.
Sommer, I., Lingenhohl, K. & Friauf, E. (1993) Principal cells of the rat medial nucleus of the trapezoid body: an intracellular in vivo study of their physiology and morphology. *Exp. Brain Res.*, **95**, 223–239.
Spirou, G.A., Brownell, W.E. & Zidanic, M. (1990) Recordings from cat trapezoid body and HRP labeling of globular bushy cell axons. *J. Neurophysiol.*, **63**, 1169–1190.
Spirou, G.A., Rager, J. & Manis, P.B. (2005) Convergence of auditory-nerve fiber projections onto globular bushy cells. *Neuroscience*, **136**, 843–863.
Taschenberger, H. & von Gersdorff, H. (2000) Fine-tuning an auditory synapse for speed and fidelity: developmental changes in presynaptic waveform, EPSC kinetics, and synaptic plasticity. *J. Neurosci.*, **20**, 9162–9173.
Thorpe, S., Delorme, A. & Van Rullen, R. (2001) Spike-based strategies for rapid processing. *Neural Netw.*, **14**, 715–725.
Tollin, D.J. (2003) The lateral superior olive: a functional role in sound source localization. *Neuroscientist*, **9**, 127–143.
Tsuchitani, C. (1997) Input from the medial nucleus of trapezoid body to an interaural level detector. *Hear. Res.*, **105**, 211–224.
Turecek, R. & Trussell, L.O. (2001) Presynaptic glycine receptors enhance transmitter release at a mammalian central synapse. *Nature*, **411**, 587–590.
Wenthold, R.J., Huie, D., Altschuler, R.A. & Reeks, K.A. (1987) Glycine immunoreactivity localized in the cochlear nucleus and superior olivary complex. *Neuroscience*, **22**, 897–912.
Wu, S.H. & Kelly, J.B. (1992) Synaptic pharmacology of the superior olivary complex studied in mouse brain slice. *J. Neurosci.*, **12**, 3084–3097.
Wu, S.H. & Kelly, J.B. (1993) Response of neurons in the lateral superior olive and medial nucleus of the trapezoid body to repetitive stimulation: intracellular and extracellular recordings from mouse brain slice. *Hear. Res.*, **68**, 189–201.
Wu, S.H. & Kelly, J.B. (1995) Inhibition in the superior olivary complex: pharmacological evidence from mouse brain slice. *J. Neurophysiol.*, **73**, 256–269.
Yin, T.C.T. (2002) Neural mechanisms of encoding binaural localization cues in the auditory brainstem. In Oertel, D., Popper, A.N. & Fay, R.R. (Eds), *Integrative Functions in the Mammalian Auditory Pathway*. Springer, New York, pp. 99–159.
Yin, T.C., Kuwada, S. & Sujaku, Y. (1984) Interaural time sensitivity of high-frequency neurons in the inferior colliculus. *J. Acoust. Soc. Am.*, **76**, 1401–1410.
Zhou, Y., Carney, L.H. & Colburn, H.S. (2005) A model for interaural time difference sensitivity in the medial superior olive: interaction of excitatory and inhibitory synaptic inputs, channel dynamics, and cellular morphology. *J. Neurosci.*, **25**, 3046–3058.